ACS APPLIED MATERIALS & INTERFACES

Research Article

www.acsami.org

Potentiostatic Reversible Photoelectrochromism: An Effect Appearing in Nanoporous $TiO_2/Ni(OH)_2$ Thin Films

Dejan Cibrev, Milena Jankulovska, Teresa Lana-Villarreal, and Roberto Gómez*

Institut Universitari d'Electroquímica i Departament de Química Física, Universitat d'Alacant, Apartat 99, E-03080 Alicante, Spain

Supporting Information

ABSTRACT: In the field of energy saving, finding composite materials with the ability of coloring upon both illumination and change of the applied electrode potential keeps on being an important goal. In this context, chemical bath deposition of $Ni(OH)_2$ into nanoporous TiO_2 thin films supported on conducting glass leads to electrodes showing both conventional electrochromic behavior (from colorless to dark brown and vice versa) together with photochromism at constant applied potential. The latter phenomenon, reported here for the first time, is characterized by fast and reversible coloration upon UV illumination. The bleaching kinetics shows first order behavior with respect to the Ni^{III} centers in the film, and an order 1.2 with respect to electrons in the TiO_2 film. From a more applied point of view, this study opens up the possibility of having two-mode smart windows showing not only conventional electrochromism but also reversible darkening upon illumination.

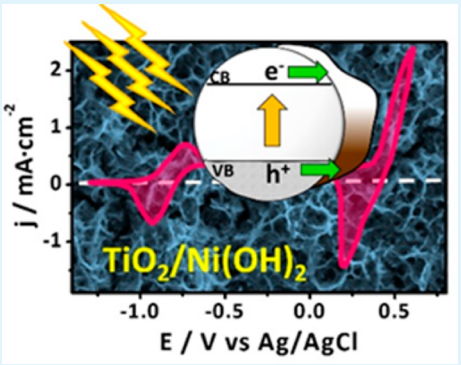

KEYWORDS: *electrochromism, photochromism, titanium dioxide, nickel hydroxide, nanoparticle*

1. INTRODUCTION

Nanostructured oxide thin films are involved in many technological applications ranging from those of environmental character to sensors or devices for converting and accumulating energy. This is a result of their particular properties, some of them related to their high porosity and surface area-to-volume ratio.[1,2] In this context, electrochromism has been intensively studied since the seminal work by Deb[3,4] in 1969, partly because it underlies the development of the so-called "smart electrochromic materials". This class of materials alters significantly and in a controlled fashion the light reflection or transmission due to a reversible coloration and bleaching induced by the application of an external potential. These promising characteristics have already led to the commercialization of electrochromic devices offering controllable light reflection or transmission in nonreflective mirrors[5−7]/nonemissive displays[8,9] or in windows.[10−13] The most successful current application of these materials is in nonreflective automotive rear-view mirrors. However, the most widely discussed potential application of electrochromic materials is in the fabrication of the so-called "smart windows", which can regulate the transmission of the incoming light due to a bias-induced color change of the material. The implementation of this technology could lead to important energy savings in buildings.[14] The generalization of these windows is hindered by the material long-term stability, the difficulty of having uniform large area coloration with good reversibility, and price. In this respect, inorganic electrochromic materials, principally oxides, compete favorably with organic and hybrid materials.

Among the inorganic electrochromic materials, $NiO/Ni(OH)_2$ is an attractive candidate due to its high electrochromic efficiency, good reversibility, and low material cost.[15,16] $NiO/Ni(OH)_2$ thin films exhibit reversible electrochromism[17−20] under applied potential due to their oxidation to NiOOH, which is accompanied by a reversible color change from colorless to dark brown/black. It is worth noting, though, that a detailed understanding of the mechanism of coloration and degradation of these films has not been attained yet, despite recent progress.[21] In any case, as the electrochromic process is associated with both electron transfer with the conducting support and ion exchange with the electrolyte, a thin nanostructured film with an increased surface area and porous structure improves the performance of the electrochromic material.[22−27] Along these lines, very recently, highly efficient electrochromic devices based on 3D nanotubular gyroid NiO networks have been prepared. Such a nanostructured NiO electrodes combine both a high surface-to-volume ratio, facilitating ion intercalation, and structural continuity, needed for electronic charge transport.[28]

Although $NiO/Ni(OH)_2$ thin films exhibit promising electrochromic properties, there is a concern about the film long-term cycling stability in alkaline media.[21] Some authors have introduced a thin film of TiO_2 between the conducting support and the $NiO/Ni(OH)_2$ film with the purpose of gaining film cycling stability.[29,30] Although the introduction of a thin TiO_2 layer is beneficial for the long-term stability of the $NiO/Ni(OH)_2$ film, the insulating properties of TiO_2 hinder the coloration contrast of the $NiO/Ni(OH)_2$ electrode.[30] A

Received: March 22, 2014
Accepted: June 13, 2014
Published: June 13, 2014

thin and porous TiO_2 film can also act as a template for the guided growth of small crystalline particles of $NiO/Ni(OH)_2$ embedded in the TiO_2 nanostructure.[31,32] In this way, one expects to obtain a structure with a lower degree of $NiO/Ni(OH)_2$ aggregation, which could be beneficial for the electrochromic process efficiency. In fact, when $NiO/Ni(OH)_2$ is oxidized to NiOOH, negative potentials have to be applied for triggering film bleaching. As NiOOH is poorly conductive,[33] the parts of the NiOOH film far away from the conducting support can lead to permanent coloration.[29,32] A porous and thin TiO_2 film could promote a growth of small $Ni(OH)_2$ particles evenly distributed over the template, which would improve the cycling reversibility of the $NiO/Ni(OH)_2$ film without sacrificing the coloration contrast.

On the other hand, it is interesting to mention that there have been some efforts devoted to oxide photochromism, although most of the inorganic systems studied so far have not exhibited enough reversibility.[34−36] In this respect, apart from being electrochromic, one would expect $TiO_2/Ni(OH)_2$ films to be photochromic. $Ni(OH)_2$ is neither a photosensitive nor a photochromic material, but coupled with TiO_2, it is susceptible to be oxidized by the holes photogenerated in TiO_2.[37] In fact, the $TiO_2/Ni(OH)_2$ composite system could promote successful charge separation of photogenerated charge carriers as demonstrated for other semiconductor composites.[38−40] In such a case, holes would be transferred to $Ni(OH)_2$ triggering its oxidation to NiOOH, and electrons would accumulate in TiO_2. In fact, it is remarkable that a $TiO_2/Ni(OH)_2$ electrode based on a compact TiO_2 layer and an electrochemically deposited $Ni(OH)_2$ overlayer exhibited weak but reversible photochromism at open circuit in contact with an alkaline aqueous solution, although the kinetics of coloration and, particularly, bleaching were quite slow.[36] The photoinduced coloration of $TiO_2/Ni(OH)_2$ thin films has been described by other authors in the context of oxidative energy storage and photoelectrochemical studies.[41−44] These studies were done with $TiO_2/Ni(OH)_2$ bilayers, being $Ni(OH)_2$ deposited on top of a TiO_2 layer, which limits to a great extent the $TiO_2/Ni(OH)_2$ interfacial area.[36,41−45] More recently, the advantages of working with a nanostructured TiO_2−$Ni(OH)_2$ film with intimate contact between both components have been put forward in the context of the UV-induced oxidative energy storage behavior.[45]

Here, we present mixed $TiO_2/Ni(OH)_2$ electrodes, composed of a nanoporous TiO_2 matrix into which $Ni(OH)_2$ is introduced by chemical bath deposition (CBD). These electrodes show reversible photoinduced electrochromism upon UV illumination when maintained at a constant potential. In the following, we refer to such a phenomenon as potentiostatic reversible photoelectrochromism (PRPEC). The nanoporous structure of the composite $TiO_2/Ni(OH)_2$ material offers an interfacial area orders of magnitude larger than in the case of compact bilayer films, allowing for the observation of PRPEC, particularly because of the improvement in the kinetics of bleaching. In this way, we are one step closer to the design of a material viable for commercial use as a photo(electro)chromic film.

2. EXPERIMENTAL SECTION

TiO_2 nanoporous films were prepared on F:SnO_2-coated transparent glass plates (FTO) from Pilkington TEC 15(15 Ω/□). TiO_2 was spin-coated on FTO plates (1000 rpm) from a dispersion containing 1 g of TiO_2 (Degussa P25, 80% anatase, 20% rutile), 30 μL of acetyl acetone (Sigma-Aldrich), 20 μL of Triton X-100 (Sigma-Aldrich), and 6 mL of ultrapure water (Millipore Elix 3). Previously, this dispersion was homogenized by sonication in an ultrasonic bath for 30 min. The spin-coated electrodes (FTO/TiO_2) were then annealed at 450 °C for 30 min. This procedure was repeated once or twice to obtain thicker electrodes. Unless otherwise stated, the TiO_2 films have a thickness of 1 μm. The as-prepared electrodes were transparent and homogeneous.

FTO/$Ni(OH)_2$ electrodes were synthesized by chemical deposition from a bath containing 25 mL of 0.5 M $NiSO_4$ (for nickel plating, Riedel-de Haën), 12.5 mL of 1 M urea (p.a, Sigma-Aldrich), and 12.5 mL of ultrapure H_2O.[46] The FTO plates were vertically supported with the conducting side against the beaker wall and the solution was heated up to 100 °C for 2 h. The deposition process is based on the fact that urea decomposes to CO_2 and NH_3 by heating at sufficiently high temperatures (90−100 °C). The Ni^{2+} cations and the hydroxide ions released by the protolytic reaction of ammonia combine creating $Ni(OH)_2$ thin films. After deposition, the samples were annealed at 200 °C in air for 1 h. The as-prepared FTO/$Ni(OH)_2$ electrodes were transparent and homogeneous. An additional characterization of the $Ni(OH)_2$ deposits can be found in ref 47.

For the preparation of FTO/TiO_2/$Ni(OH)_2$ or FTO/$Ni(OH)_2$/TiO_2 electrodes, $Ni(OH)_2$ was deposited on FTO/TiO_2 or TiO_2 was spin-coated on FTO/$Ni(OH)_2$ electrodes, respectively. The as-prepared mixed film electrodes were also transparent and homogeneous. In the context of this study, it is relevant that the thickness of the TiO_2 /$Ni(OH)_2$ films was 1.3 μm. After dissolving the $Ni(OH)_2$ layer with a concentrated HCl solution, the thickness was reduced to 1 μm.

Electrochemical experiments were performed at room temperature in a standard electrochemical cell connected to a computer-controlled Autolab PGSTAT 30 potentiostat with an N_2-purged 1 M NaOH solution employed as an electrolyte. All potentials were measured against and are referred to an Ag/AgCl/KCl(sat) reference electrode, whereas a Pt wire was used as a counter electrode. Illumination was carried out by means of a 300 W Xe arc lamp (Oriel) equipped with a water filter (irradiance: 800 $mW{\cdot}cm^{-2}$). Spectroelectrochemical measurements were performed by coupling an electrochemical cell to a UV−vis spectrophotometer (UV-2401 PC Shimadzu). The cell employed for the spectroelectrochemical measurements was equipped with a cuvette fitted at its bottom and mounted on the support of the spectrophotometer sample chamber. The reference and the counter electrode are the same as in the case of the conventional electrochemical cell described above. The experiments were conducted by coupling chronoamperometric measurements at several potentials with absorbance measurements. In the case of the spectroelectrochemical measurements under illumination, the working electrode (FTO/TiO_2/$Ni(OH)_2$) was fixed in a position perpendicular to the probe beam while illuminated by a diode laser Oxxius (λ = 375 nm, W = 7 mW) at an oblique angle of incidence (see Figure S1 in the Supporting Information).

The morphology and compositional mapping of the TiO_2 electrodes, prior and after decoration with $Ni(OH)_2$, was characterized using field emission scanning electron microscopy (FE-SEM, Zeiss model MERLIN). This microscope was equipped with an X-ray detector for microanalysis (energy dispersive X-ray spectroscopy, EDS) and mapping. The images were obtained using either an in-lens detector or a conventional secondary electron detector. The composition of the electrodes was also studied by X-ray photoelectron spectroscopy (XPS) using a Kα Thermoscientific spectrometer, equipped with an Ar ion sputter gun to perform depth profile analysis. Ta_2O_5 was used as a reference to calculate the depth.

The topography of the TiO_2 and $Ni(OH)_2$ films was evaluated by means of tapping mode atomic force microscopy (AFM), using a Nanoscope III (Digital instruments) operated at room temperature in air. Film thickness was measured by means of an Alpha Step D-100 profilometer.

3. RESULTS AND DISCUSSION

This section is organized as follows. First of all, the morphological and chemical characterization of $TiO_2/Ni(OH)_2$ films by means of SEM and XPS is presented, and then, their electrochemical and electrochromic behavior is briefly discussed. Next, the electrochemical behavior under illumination is discussed on the basis of cyclic voltammetry and photocurrent and photopotential transients. Finally, spectroelectrochemical experiments are shown to quantitatively study the photoelectrochromic effect.

Figure 1 shows FE-SEM cross-sectional (a,b) and top views (c,d) of TiO_2 thin films before (a,c) and after (b,d) deposition

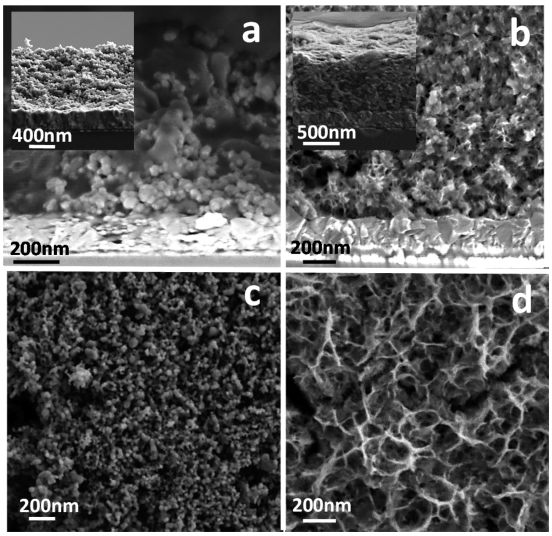

Figure 1. FE-SEM images for a TiO_2 thin film prior (a and c) and after deposition of $Ni(OH)_2$ for 2 h (b and d): cross section (a and b) and top view (c and d). The insets in panels a and b show the film thickness and were obtained with a conventional secondary electron detector. Images in panels a and b were obtained with an in-lens detector.

of $Ni(OH)_2$ for 2 h. Parts a and b of Figure 1 show the cross-sectional images obtained with the in-lens detector, while the corresponding insets were obtained with the conventional secondary electron detector. With the in-lens detector, images revealing differences in the work function, with high contrast and lateral resolution, can be obtained. Prior to $Ni(OH)_2$ deposition, the TiO_2 showed the typical morphology of a nanoparticulate electrode, both in cross-sectional and top views, constituted by nanoparticles of 20−30 nm in diameter together with much larger particles or aggregates (hundreds of nanometeres in size). After $Ni(OH)_2$ deposition, the cross-sectional view changes substantially, showing a higher degree of compactness. The view in Figure 1b clearly indicates that $Ni(OH)_2$ flakes are formed in most of the void space of the TiO_2 nanoporous layers. These flakes can also be seen covering all the surface in the top view of the $TiO_2/Ni(OH)_2$ thin film (Figure 1d). These results indicate that the deposition of the $Ni(OH)_2$ particles occurs both in the interior of the porous TiO_2 matrix and as an overlayer (see Figure S2 in the Supporting Information for an illustrative cross-section). AFM images obtained for TiO_2 and $Ni(OH)_2$ films show features very similar to those appearing in Figure 1c,d (see Figure S3 in the Supporting Information). It is worth mentioning that the $Ni(OH)_2$ nanostructure (both on FTO and on FTO/TiO_2) shows a typical morphology,[19,22] highly porous, and apparently formed by flakes with large and open voids, which facilitates its interaction with the electrolyte.

Figure 2a shows a SEM cross-sectional image for the $FTO/TiO_2/Ni(OH)_2$ sample together with the EDS microanalysis

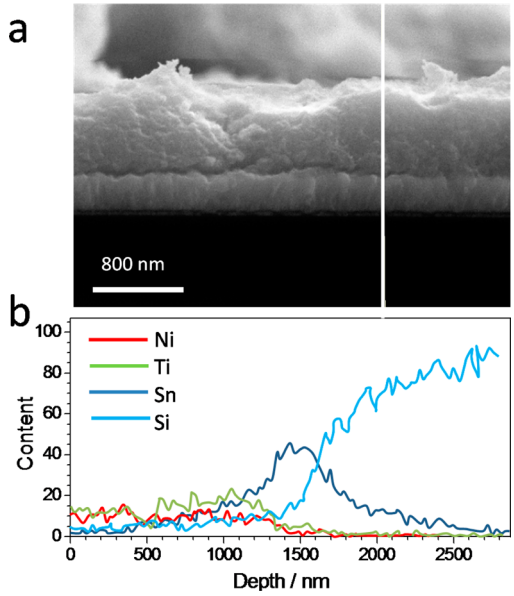

Figure 2. FE-SEM cross section view for a TiO_2 electrode modified with $Ni(OH)_2$ (a) and the composition along the white line indicated in part a (b).

performed along the line marked in Figure 2a for Ni, Ti, Sn, and Si (Figure 2b). It is clearly seen that, apart for the predominance of Sn and Si for high values of the depth (corresponding to the FTO layer and glass substrate, respectively), Ni accompanies Ti throughout the whole thickness of the film, which attests the intimate contact between TiO_2 and $Ni(OH)_2$. Figure 3 corresponds to the Ti/

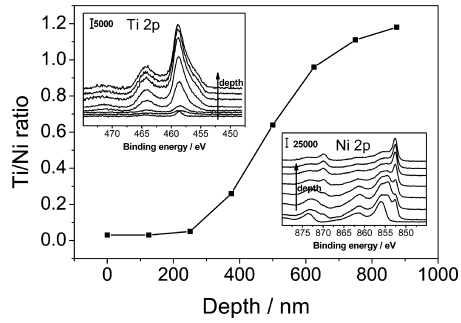

Figure 3. Ti/Ni atomic ratio obtained from XPS measurements as a function of the depth for a TiO_2 electrode modified with $Ni(OH)_2$. The insets show the corresponding Ni 2p and Ti 2p XPS high resolution spectra.

Ni atomic ratio for an $FTO/TiO_2/Ni(OH)_2$ sample as obtained from integration of XPS measurements for the Ni 2p and Ti 2p bands (see the insets for the corresponding high resolution spectra) done as a function of depth. These XPS depth profiling results are in full agreement with the SEM/EDS results presented above. The films being investigated are thus constituted by a composite layer of $TiO_2/Ni(OH)_2$, together with an outer layer of pure $Ni(OH)_2$ around 300 nm in

thickness. Note that the strong shift observed in the Ni 2p spectra is due to the reduction of Ni^{II} to Ni^0 as a results of Ar^+ ion bombardment.[48]

Voltammetric experiments were done with the FTO/TiO_2/$Ni(OH)_2$ electrodes to characterize their electrochemical and electrochromic behavior (Figure 4). For the sake of

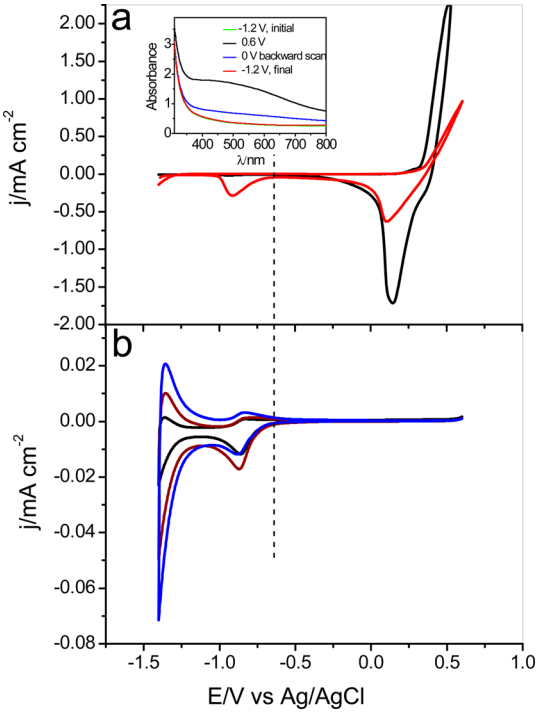

Figure 4. (a) CVs for FTO/$Ni(OH)_2$ (black curve) and FTO/TiO_2/$Ni(OH)_2$ (red curve) electrodes. The $Ni(OH)_2$ deposition time used in both cases was the same (2 h). Scan rate = 20 mV/s. (b) CVs in the dark for an FTO/TiO_2 electrode with one (black curve), two (red curve), and three (blue curve) layers of TiO_2 deposited by spin coating. The dashed line is included as a guide for the eye. Scan rate = 10 mV/s. Inset: Absorbance spectra for an FTO/TiO_2/$Ni(OH)_2$ electrode at different potentials.

comparison, experiments were also performed with an FTO/$Ni(OH)_2$ electrode. The cyclic voltammogram (CV) for an FTO/$Ni(OH)_2$ electrode, apart from a small capacitative current in a wide potential region (from −1.4 to 0 V), shows as the main feature a pair of peaks associated with the oxidation of $Ni(OH)_2$ to NiOOH and its subsequent reduction, accompanied by the corresponding coloration and bleaching. A similar behavior has been previously reported by us[47] and other groups.[19,22]

TiO_2/$Ni(OH)_2$ electrodes show an electrochemical/electrochromic behavior similar to that of $Ni(OH)_2$. However, an additional reduction peak appears at around −0.9 V (see red curve in Figure 4a). It is remarkable that in the potential range between −0.6 and 0 V, FTO/$Ni(OH)_2$ electrodes are colorless as all the NiOOH particles have been reduced back to $Ni(OH)_2$, while FTO/TiO_2/$Ni(OH)_2$ electrodes keep a significant brown coloration, which is an indication that NiOOH is still present.

A series of UV−vis absorbance spectra for an FTO/TiO_2/$Ni(OH)_2$ electrode recorded at different potentials are shown in the inset of Figure 4a. As observed, the film is fully colored at 0.6 V and fully bleached at −1.2 V and shows a reversible behavior. The fully colored state is characterized by a broad absorption throughout the whole visible range, which is higher at shorter wavelengths (dark brown color). In agreement with the visual observations described above, lowering the applied potential from 0.6 to 0 V does not trigger a complete bleaching of the electrode, which keeps a significant brown coloration (see also Figure S4 in the Supporting Information). In this respect, we hypothesize that the peak appearing at −0.9 V is due to the reduction of the NiOOH not in direct contact with the FTO substrate but in intimate contact with TiO_2. As indicated above, SEM and XPS results (see Figures 2 and 3) provide direct evidence that $Ni(OH)_2$ is evenly distributed throughout the TiO_2 nanostructure.

The fact that the reduction of NiOOH particles occurs at more negative potentials when they are not in direct contact with the substrate, indicates that the electrochemical characteristics of the TiO_2/$Ni(OH)_2$ mixed films are partly determined by the electrochemical properties of the TiO_2 nanoporous substrate. As observed for TiO_2 electrodes of different thickness (Figure 4b), the accumulation region, in which TiO_2 layers are conductive,[49,50] appears at potentials more negative than −0.6 V. As TiO_2 is not intentionally doped, it behaves as an insulator at potentials above −0.6 V.[51] This means that it cannot sustain any electrochemical reaction in the dark at potentials higher than −0.6 V. As water is oxidized on FTO in the upper potential range, either the evolved oxygen or intermediate oxidizing species could chemically oxidize the $Ni(OH)_2$ not in direct contact with FTO. In this way, NiOOH would be generated in spite of not being in direct contact with a conducting phase. In the subsequent negative-going scan, the NiOOH in contact with FTO is easily reduced, whereas that in contact only with TiO_2 keeps on being oxidized until electrons are injected into the TiO_2 at potentials lower than −0.6 V. At this point, the conductivity of TiO_2 increases and can mediate the reduction of NiOOH to $Ni(OH)_2$.

In the following, we analyze the photoelectrochemical behavior of FTO/TiO_2/$Ni(OH)_2$ electrodes in comparison with that of FTO/TiO_2 electrodes (Figure 5). The latter show the typical sigmoidal voltammetric curve under illumination with an onset potential at around −0.9 V for the photocurrent (j_{ph}), which is attributed to the oxidation of water (green curve in Figure 5a). As seen in Figure 5a, introducing $Ni(OH)_2$ into the TiO_2 matrix changes the morphology of the j_{ph} vs E curve. A well-defined photo-oxidation peak is observed at around −0.7 V, absent in the case of the blank FTO/TiO_2 sample. In addition, the photocurrent onset shifts negatively by 0.1 V upon the presence of $Ni(OH)_2$. These observations indicate that the oxidation of $Ni(OH)_2$ is favored over that of water. In fact, the development of the photocurrent coincides with the appearance of a brown spot in the region of the electrode submitted to illumination (inset in Figure 5a). This indicates that at FTO/TiO_2/$Ni(OH)_2$ electrodes, the oxidation of $Ni(OH)_2$ to NiOOH occurs at potentials much more negative (by 1.2 V) than in the dark (red curve). It should be stressed that FTO/$Ni(OH)_2$ electrodes do not show any photoeffect.

Figure 5b shows the UV−visible absorbance spectra for an FTO/TiO_2/$Ni(OH)_2$ electrode in the bleached state (at −0.75 V) and after exposure to 375 nm light for 10 min at the same potential. As observed this long-term exposure to light leads to a coloration of the electrode due to the photooxidation of the $Ni(OH)_2$ not in direct contact with the FTO substrate (but in direct contact with the TiO_2). It is worth noting that this spectrum is almost identical to that obtained after the partial

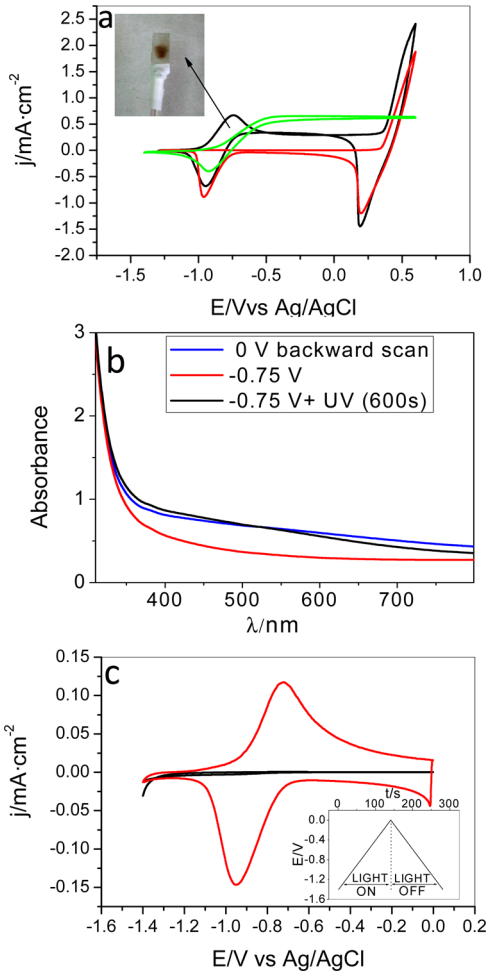

Figure 5. (a) CVs for FTO/TiO_2/$Ni(OH)_2$ electrodes in the dark (red curve) and under illumination (black curve). A peak at around −0.9 V is observed associated with photoinduced electrochromism (black curve) absent in the CVs under illumination for the blank FTO/TiO_2 electrode (green curve); the inset shows a picture of the electrode colored in the region submitted to illumination. Scan rate = 20 mV/s. (b) Absorption spectra obtained at 0 V in the backward scan (after scanning the potential up to 0.6 V) and at −0.75 V before and after UV illumination (375 nm) for 10 min. (c) Voltammetric scans in the dark (black curve) and under illumination during the positive-going scan and in the dark in the subsequent negative-going scan (red curve) for the composite TiO_2/$Ni(OH)_2$ mixed film; the inset shows the potential/illumination program. Scan rate = 10 mV/s.

bleaching of the electrode that results from changing the potential from 0.6 to 0 V.

In the following, we propose a mechanism for the coloration of the electrode upon its illumination at constant potential. As proposed previously,[36] illumination triggers the generation of electrons and holes in TiO_2. The photogenerated holes can be transferred to the $Ni(OH)_2$ particles, provoking their oxidation to NiOOH according to

$$Ni(OH)_2(s) + OH^-(aq) + h^+(TiO_2) \rightarrow NiOOH(s) + H_2O(l) \quad (1)$$

The experiment in Figure 5c adds further evidence for this notion. The red curve shows a positive-going voltammetric scan performed under illumination for an FTO/TiO_2/$Ni(OH)_2$ electrode, followed by a subsequent negative-going scan in the dark (see inset in Figure 5c for the potential/illumination program). The black curve shows that for a voltammetric cycle recorded in the dark, only a small capacitive signal is observed. As expected, when the positive−going scan is performed under illumination, the photocurrent peak corresponding to the oxidation of $Ni(OH)_2$ appears. Importantly, the subsequent dark negative−going scan shows a peak corresponding to the reduction of NiOOH as confirmed by the bleaching of the electrode. The fact that the charges under the cathodic and anodic peaks are similar clearly indicates that, in the potential range used in this experiment, the photooxidation of water does not interfere with that of $Ni(OH)_2$. Importantly, the voltammetric peaks show a relatively high degree of reversibility, opening up the possibility of having $Ni(OH)_2$ photooxidation and subsequent NiOOH reduction occurring at a constant potential.

From the locations of the band edges of TiO_2, together with the equilibrium electrode potentials for the redox couples NiOOH/$Ni(OH)_2$ and O_2/H_2O at pH = 14 (see Figure 6),[51,52]

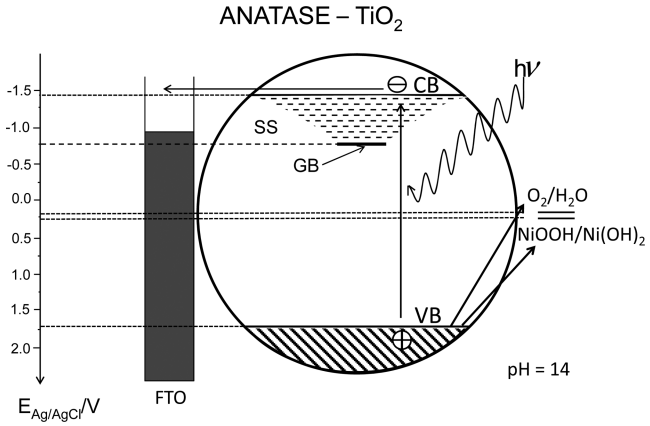

Figure 6. Scheme of the valence and conduction band positions for TiO_2 together with those for the grain boundary (GB) and surface states (SS) with respect to the potentials of the NiOOH/$Ni(OH)_2$ and O_2/H_2O redox pairs at pH = 14.

it is evident that the photogenerated holes in TiO_2 are thermodynamically capable of oxidizing both $Ni(OH)_2$ and H_2O. Actually, the driving forces for the oxidation of $Ni(OH)_2$ and H_2O are virtually the same, and therefore the preference for $Ni(OH)_2$ oxidation is mainly kinetic in origin. It is worth noting that in our case the prevalence of field-driven electron−hole separation as proposed by other authors[45] is not plausible, mainly because the dimension of the nano-objects of both TiO_2 and $Ni(OH)_2$ does not allow for the existence of an electric field when the thin film is permeated by the electrolyte as in the present case.

Open circuit potential (OCP) experiments measured under interrupted illumination provide additional information on the charge separation process at the TiO_2/$Ni(OH)_2$ interface. Figure 7 shows these measurements for FTO/TiO_2/$Ni(OH)_2$ and FTO/$Ni(OH)_2$/TiO_2 electrodes. In the former case, upon illumination there is a sudden decrease of the OCP, which indicates that part of the holes photogenerated in the TiO_2 are transferred to the $Ni(OH)_2$, triggering its oxidation to NiOOH and the rest are trapped at the TiO_2 surface or recombine with photogenerated electrons (Figure 7a). The equilibration between the quasi-Fermi level of electrons in TiO_2 and the Fermi level of FTO leads to the observed behavior. Upon light

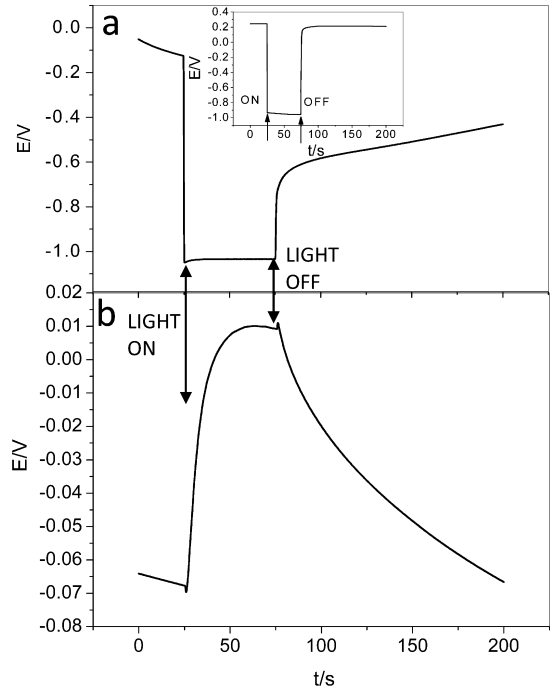

Figure 7. (a) Transient photopotential measurements for an FTO/TiO_2/$Ni(OH)_2$ electrode in an N_2-purged 1 M NaOH solution. Inset: The corresponding experiment for an air-saturated electrolyte solution. (b) Transient photopotential measurements for an FTO/$Ni(OH)_2$/TiO_2 electrode in contact with an N_2-purged 1 M NaOH solution.

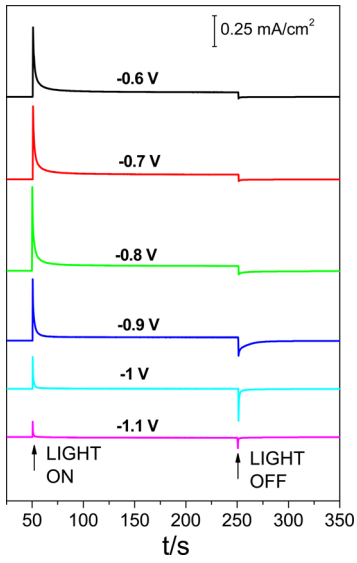

Figure 8. Chronoamperometric curves under transient illumination at different potentials for an FTO/TiO_2/$Ni(OH)_2$ electrode in contact with N_2-purged 1 M NaOH.

interruption, the accumulated electrons may reduce NiOOH back to $Ni(OH)_2$:

$$NiOOH(s) + e^-(TiO_2) + H_2O \rightarrow Ni(OH)_2(s) + OH^-(aq) \quad (2)$$

This consumption of electrons leads to an increase of the OCP. The change in OCP upon illumination is much faster than its relaxation upon light interruption, which indicates that bleaching is much slower than coloration. In contrast, in the presence of oxygen, the OCP relaxation becomes much faster (See inset in Figure 7a), showing that photogenerated TiO_2 electrons are primarily consumed in reducing O_2[53,54] instead of being employed in the reduction of NiOOH, which hinders the bleaching process. Importantly, these results indicate that, in the absence of oxygen, these films should sustain a significant reversible photochromism, while in its presence, bleaching would not occur.

The experiments done with an FTO/$Ni(OH)_2$/TiO_2 electrode support the preceding discussion. Because in this case $Ni(OH)_2$ is directly attached to FTO, the OCP value is a probe of the oxidation state of the Ni hydr(oxide) layer. The transfer of the holes photogenerated in the TiO_2 to the underlying $Ni(OH)_2$ results in its partial oxidation and, therefore, in the observed increase of the OCP. Upon interruption of the illumination, the OCP decreases, indicating that Ni^{III} is reduced back to Ni^{II} by the electrons accumulated in the TiO_2. Importantly, the similar kinetics of electron consumption in the TiO_2, and of NiOOH reduction deduced from the relaxations of the OCP in Figures 7a and 7b, respectively, indicate that no significant interference from other redox processes occurs in the absence of oxygen.

In order to check the possibility of having PRPEC, we performed a series of chronoamperometric experiments at different applied potentials under interrupted illumination for FTO/TiO_2/$Ni(OH)_2$ electrodes (Figure 8). For all the studied potentials, an anodic spike appears upon illumination whose height grows as the applied potential becomes less negative until −0.8 V. For potentials above −0.8 V the height of the spike is approximately constant. This signal is associated with the oxidation of $Ni(OH)_2$ (and possibly water). When the illumination is interrupted, a cathodic spike appears corresponding to the reduction of the NiOOH generated upon illumination. This spike tends to disappear as the potential increases, which indicates that the kinetics of the bleaching process becomes increasingly sluggish. Importantly, in the potential range between −1.0 and −0.8 V, the charges under the anodic and cathodic spikes are similar. This is the potential range in which one would expect reversible photoelectrochromism.

For a further study of the PRPEC (its coloration contrast and bleaching), it is essential to measure light absorption as a function of time upon interrupted illumination at different potentials for an FTO/TiO_2/$Ni(OH)_2$ electrode. Figure 9a shows that upon illumination of the film, a fast increase of the absorbance at 500 nm takes place. This indicates that the $Ni(OH)_2$ oxidation kinetics is rather fast, full coloration being achieved in a few tens of seconds in agreement with the chronoamperometric and OCP experiments shown above. As observed, the kinetics of coloration does not depend significantly on applied potential, in contrast with that of the bleaching process.

In order to analyze more quantitatively the bleaching kinetics, let us assume, as suggested by eq 2, that the bleaching process is first-order with respect to the concentration of Ni^{III} centers in the film ($[Ni^{III}]$):

$$-\frac{d[Ni^{III}]}{dt} = k[Ni^{III}] \quad (3)$$

where k is the first-order rate constant for the bleaching process. By assuming that the absorbance at 500 nm ($A(t)$) is

dx.doi.org/10.1021/am5017396 | ACS Appl. Mater. Interfaces 2014, 6, 10304−10312

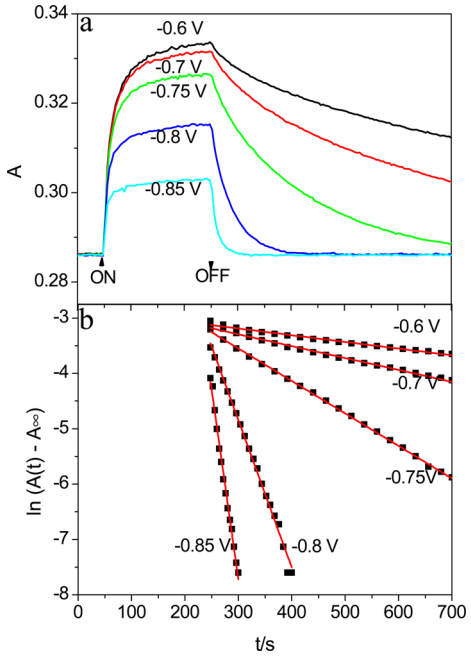

Figure 9. (a) Absorbance at 500 nm vs time for an FTO/TiO_2/$Ni(OH)_2$ electrode maintained at different potentials. In the first 50 s, absorbance was measured in the dark; then, the film was illuminated for 200 s and finally the light was turned off. (b) Plot of $\ln(A(t) - A_\infty)$ vs time for different applied potentials.

directly proportional to $[Ni^{III}]$, the integration of the rate law (eq 3) leads to

$$\ln(A(t) - A_\infty) = \ln(A_0 - A_\infty) - kt \quad (4)$$

where A_0 and A_∞ are the initial and final values of the absorbance, respectively. Equation 4 indicates that a plot of $\ln(A(t) - A_\infty)$ vs t should be linear. In fact, the corresponding plots shown in Figure 9b confirm that the bleaching process is first order with respect to Ni^{III}. However, the fact that depending on the applied potential, the slopes of the different lines change indicates that k is a function of the applied potential. Actually, this constant varies almost 2 orders of magnitude for a change in the applied potential of around 250 mV (Figure 10).[50] This observation relates to the fact that in these experiments the concentration of electrons is not time-dependent, but instead, it is determined by the applied potential; that is, electrons are replenished in the TiO_2 nanostructure from the conductive substrate much faster than they are consumed in the relatively slow bleaching process. Importantly, in such a case, by integrating the voltammetric profile in Figure 4b for the corresponding film thickness between the onset of the accumulation region (around −0.6 V) and the applied potential, the actual electron concentration in the nanostructured TiO_2 film for each of the experiments shown in Figure 9 can be obtained. Once the stationary concentration of electrons is known as a function of the applied potential, the bleaching process order with respect to the electrons can be determined.[55] In fact, by assuming that the apparent first-order rate constant is proportional to the concentration of electrons (n):

$$k = k' n^\alpha \quad (5)$$

$$\ln k = \ln k' + \alpha \ln n$$

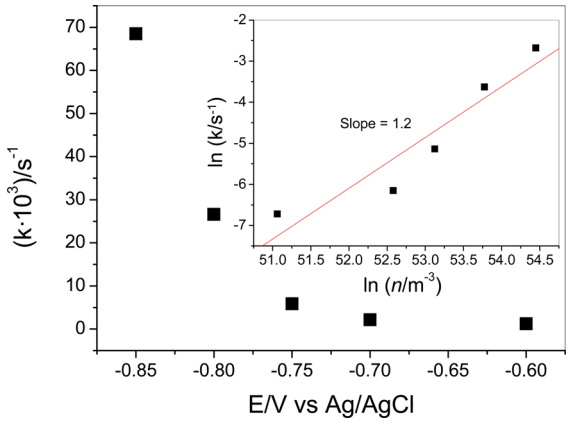

Figure 10. Apparent rate constant for the bleaching process for an FTO/TiO_2/$Ni(OH)_2$ mixed electrode as a function of the applied potential. Inset: Plot of ln k vs ln n; the slope of this curve represents the order of the bleaching reaction with respect to the concentration of CB + SS + GB electrons in TiO_2 at different potentials.

it is deduced that a plot of ln k vs ln n should be linear, with the slope providing the reaction order with respect to the electrons. The experimental data shown in Figure 10 indicate that eq 5 is followed in an approximate way and that the order with respect to the electrons is close to 1, more precisely 1.2. For rationalizing such a value, it should be taken into account that not all the TiO_2 electrons are equivalent because (in the case of anatase) they are located at grain boundaries (GB) and at surface states (SS) of increasing energy (see Figure 6) as we increase their concentration.[51,56] Therefore, adherence to simple rate laws cannot be but approximate.

Based on the previous discussion, the mechanism proposed for the PRPEC can be summarized as follows. Upon illumination, holes are generated in the valence band of TiO_2. As the holes have enough oxidative power, they can be transferred either to H_2O or to $Ni(OH)_2$. The transfer to $Ni(OH)_2$ seems to be favored by kinetic reasons. A photostationary state is finally reached in which the concentration of electrons in the TiO_2 is dictated by the applied potential and that of holes in the nickel hydr(oxide) phase is limited by recombination with the electrons in TiO_2. Upon light interruption, no more holes are generated and recombination of holes in the nickel hydr(oxide) phase with electrons in the TiO_2 prevails, which leads to the bleaching of the film. This potentiostatic phenomenon only occurs in a limited range of applied potentials. In fact, below this range, the concentration of electrons in the TiO_2 is very large and no holes can be transferred to $Ni(OH)_2$ (the potential would be lower than the onset potential of TiO_2). Above this range, the concentration of electrons in the TiO_2 is too small and no bleaching occurs after interruption of illumination.

From a practical point of view, two obvious advantages of the PRPEC over open circuit photochromism are that the coloration contrast achieved is potentially much higher and, more importantly, that the supply of electrons from the conducting substrate makes the bleaching much faster. The charge separation ability of the FTO/TiO_2/$Ni(OH)_2$ electrodes and, in turn, their photoelectrochromic performance, depends essentially on the structure of the mixed film, more precisely on the extent of intimate contact between TiO_2 and $Ni(OH)_2$ particles. The nanoporous TiO_2 matrix offers the possibility of substantial $Ni(OH)_2$ deposition inside its

structure, which gives rise to an increased interfacial TiO_2–$Ni(OH)_2$ area in comparison with a compact $TiO_2/Ni(OH)_2$ bilayer film. Thus, the nanoporous structure of the $TiO_2/Ni(OH)_2$ film offers the possibility of a better reversibility without sacrificing the contrast, which could be increased by preparing thicker nanoporous mixed films. Optimizing the $TiO_2/Ni(OH)_2$ structure by modifying the TiO_2 nanoporous matrix from a disordered 3-D structure into a more ordered one,[57] and changing the way of depositing $Ni(OH)_2$ are tasks that are underway in our laboratory to improve the PRPEC behavior.

4. CONCLUSION

In this work, we have introduced a new effect in the field of photo(electro)chromism: the PRPEC (Potentiostatic Reversible PhotoElectroChromism). Mixed $TiO_2/Ni(OH)_2$ thin nanoporous films supported on conducting glass and maintained at constant potential get colored upon shining on them UV light, fully bleaching when illumination is interrupted. The value of the applied constant potential allows one to finely tune both the coloration contrast and the bleaching kinetics, in such a way that a convenient trade off can be found between these factors. The phenomenon is possible because of the existence of an extended $TiO_2/Ni(OH)_2$ interfacial area facilitated by a nanoporous structure with intimate contact between the components. It is remarkable that working with this type of substrate has enormously helped in the elucidation of the rate law for the bleaching process, which roughly follows a first order kinetics for both electrons (the order for electrons is actually 1.2) and Ni^{III} centers in the nickel (hydr)oxide deposit. From an applied point of view, we believe that our results could facilitate the development of smart windows with a new functionality because, in addition to the conventional electrochromic effect, they would work in a second mode, in which, at a constant applied bias, the coloration would respond to the incident light intensity.

■ ASSOCIATED CONTENT

Supporting Information

Sketch of the electrochemical cell for photospectroelectrochemical UV–vis measurements (Figure S1), a SEM cross-sectional view of an $FTO/TiO_2/Ni(OH)_2$ electrode (Figure S2), AFM images for the TiO_2 and $Ni(OH)_2$ surfaces (Figure S3), and UV–vis spectroelectrochemical measurements in the dark for an $FTO/TiO_2/Ni(OH)_2$ electrode (Figure S4). This material is available free of charge via the Internet at http://pubs.acs.org/.

■ AUTHOR INFORMATION

Corresponding Author

*Phone: +34 965903748. E-mail: Roberto.Gomez@ua.es.

Notes

The authors declare no competing financial interest.

■ ACKNOWLEDGMENTS

This work was financially supported by the Spanish Ministry of Economy and Competitiveness (MINECO) through project MAT2012-37676 (FONDOS FEDER). M.J. and D.C. also thank the Spanish MINECO for the award of FPI grants.

■ REFERENCES

(1) Li, J.; Zhang, J. Z. Optical Properties and Applications of Hybrid Semiconductor Nanomaterials. *Coord. Chem. Rev.* **2009**, *253*, 3015–3041.
(2) Granqvist, C. G.; Azens, A.; Hesler, P.; Kish, L. B.; Österlund, L. Nanomaterials for Benign Indoor Environments: Electrochromics for "Smart Windows", Sensors for Air Quality, and Photocatalysts for Air Cleaning. *Sol. Energy Mater. Sol. Cells* **2007**, *91*, 355–365.
(3) Deb, S. K. A Novel Electrophotographic System. *Appl. Opt. Suppl.* **1969**, *3*, 192–195.
(4) Deb, S. K. Optical and Photoelectric Properties and Color Centers in Thin Films of Tungsten Oxide. *Philos. Mag.* **1973**, *27*, 801–822.
(5) Bange, K.; Gambke, T. Electrochromic Materials for Optical Switching Devices. *Adv. Mater.* **1992**, *2*, 10–16.
(6) Baucke, F. G. K. Electrochromic Mirrors with Variable Reflectance. *Sol. Energy Mater.* **1987**, *16*, 67–77.
(7) Baucke, F. G. K.; Bange, K.; Gambke, T. Reflecting Electrochromic Devices. *Displays* **1988**, *9*, 179–187.
(8) Coleman, J. P.; Lynch, A. T.; Madhukar, P.; Wagenknecht, J. H. Antimony-Doped Tin Oxide Powders: Electrochromic Materials for Printing Displays. *Sol. Energy Mater. Sol. Cells* **1999**, *56*, 395–418.
(9) Edwards, M. O. M.; Boschloo, G.; Gruszecki, T.; Pettersson, H.; Sohlberg, R.; Hagfeldt, A. Electric-Paint Displays with Carbon Counter Electrodes. *Electrochim. Acta* **2001**, *46*, 2187–2193.
(10) Granqvist, C. G.; Azens, A.; Isidorsson, J.; Kharrazi, M.; Kullman, L.; Lindstrom, T.; Niklasson, G. A.; Ribbing, C. G.; Rönnow, D.; Strømme Mattson, M.; Veszelei, M. Towards the Smart Window: Progress in Electrochromics. *J. Non-Cryst. Solids* **1997**, *218*, 273–279.
(11) Rauh, R. D. Electrochromic Windows: an Overview. *Electrochim. Acta* **1999**, *44*, 3165–3176.
(12) Bell, J. M.; Skryabin, I. L.; Matthews, J. P. In *Encyclopedia of Smart Materials*; Schwartz, M., Eds.; Wiley: New York, 2002; Vol. 2, pp 1134–1145.
(13) Azens, A.; Granqvist, C. G. Electrochromic Smart Windows: Energy Efficiency and Device Aspects. *J. Solid State Electrochem.* **2003**, *7*, 64–68.
(14) Niklasson, G. A.; Granqvist, C. G. Electrochromics for Smart Windows: Thin Films of Tungsten Oxide, and Devices Based on These. *J. Mater. Chem.* **2007**, *17*, 127–156.
(15) Granqvist, C. G. Solar Energy Materials. *Adv. Mater.* **2003**, *15*, 1789–1803.
(16) Avendano, E.; Berggren, L.; Niklasson, G. A.; Granqvist, C. G.; Azens, A. Electrochromic Materials and Devices: Brief Survey and New Data on Optical Absorption in Tungsten Oxide and Nickel Oxide Films. *Thin Solid Films* **2006**, *496*, 30–36.
(17) Nakaoka, K.; Ueyama, J.; Ogura, K. Semiconductor and Electrochromic Properties of Electrochemically Deposited Nickel Oxide Films. *J. Electroanal. Chem.* **2004**, *571*, 93–99.
(18) Abe, Y.; Lee, S.-H.; Zayim, E. O.; Tracy, C. E.; Pitts, J. R.; Deb, S. K. Electrochromic Properties of Ni Oxide Thin Films in Diluted Acidic Electrolytes and Their Stability. *Sol. Energy Mater. Sol. Cells* **2008**, *92*, 160–163.
(19) Sonavane, A. C.; Inamdar, A. I.; Shinde, P. S.; Deshmukh, H. P.; Patil, R. S.; Patil, P. S. Efficient Electrochromic Nickel Oxide Thin Films by Electrodeposition. *J. Alloys Compd.* **2010**, *489*, 667–673.
(20) Huang, H.; Tian, J.; Zhang, W. K.; Gan, Y. P.; Tao, X. Y.; Xia, X. H.; Tu, J. P. Electrochromic Properties of Porous NiO Thin Film as a Counter Electrode for NiO/WO_3 Complementary Electrochromic Window. *Electrochim. Acta* **2011**, *56*, 4281–4286.
(21) Ren, Y.; Chim, W. K.; Guo, L.; Tanoto, H.; Pan, J.; Chiam, S. Y. The Coloration and Degradation Mechanisms of Electrochromic Nickel Oxide. *Sol. Energy Mater. Sol. Cells* **2013**, *116*, 83–88.
(22) Xia, X. H.; Tu, J. P.; Zhang, J.; Wang, X. L.; Zhang, W. K.; Huang, H. Electrochromic Properties of Porous NiO Thin Films Prepared by a Chemical Bath Deposition. *Sol. Energy Mater. Sol. Cells* **2008**, *92*, 628–633.
(23) Yuan, Y. F.; Xia, X. H.; Wu, J. B.; Chen, Y. B.; Yang, J. L.; Guo, S. Y. Enhanced Electrochromic Properties of Ordered Porous Nickel

Oxide Thin Film Prepared by Self-assembled Colloidal Crystal Template-Assisted Electrodeposition. *Electrochim. Acta* **2011**, *56*, 1208−1212.
(24) Cai, G. F.; Gu, C. D.; Zhang, J.; Liu, P. C.; Wang, X. L.; You, Y. H.; Tu, J. P. Ultra-fast Electrochromic Switching of Nanostructured NiO Films Electrodeposited from Choline Chloride-based Ionic Liquid. *Electrochim. Acta* **2013**, *87*, 341−347.
(25) Cao, F.; Pan, G. X.; Xia, X. H.; Tang, P. S.; Chen, H. F. Hydrothermal-Synthesized Mesoporous Nickel Oxide Nanowall Arrays with Enhanced Electrochromic Application. *Electrochim. Acta* **2013**, *111*, 86−91.
(26) Sialvi, M. Z.; Mortimer, R. J.; Wilcox, G. D.; Teridi, A. M.; Varley, T. S.; Wijayantha, K. G. U.; Kirk, C. A. Electrochromic and Colorimetric Properties of Nickel(II) Oxide Thin Films Prepared by Aerosol-Assisted Chemical Vapor Deposition. *ACS Appl. Mater. Interfaces* **2013**, *5*, 5675−5682.
(27) Chiang, K.-K.; Wu, J.-J. Fuel-Assisted Solution Route to Nanostructured Nickel Oxide Films for Electrochromic Device Application. *ACS Appl. Mater. Interfaces* **2013**, *5*, 6502−6507.
(28) Scherer, M. R. J.; Steiner, U. Efficient Electrochromic Devices Made from 3D Nanotubular Gyroid Networks. *Nano Lett.* **2013**, *13*, 3005−3010.
(29) Al-Kahlout, A.; Pawlicka, A.; Aegerter, M. A. Brown Coloring Electrochromic Devices Based on NiO−TiO_2 Layers. *Sol. Energy Mater. Sol. Cells* **2006**, *90*, 3583−3601.
(30) Martini, M.; Brito, G. E. S.; Fantini, M. C. A.; Craievich, A. F.; Gorenstein, A. Electrochromic Properties of NiO-Based Thin Films Prepared by Sol−Gel and Dip Coating. *Electrochim. Acta* **2001**, *46*, 2275−2279.
(31) Baudry, P.; Rodrigues, A. C. M.; Aegerter, M. A. Dip-coated TiO_2−CeO_2 Films as Transparent Counter Electrode for Transmissive Electrochromic Device. *J. Non-Cryst. Solids* **1990**, *121*, 319−322.
(32) Al-Kahlout; Heusing, S.; Aegerter, M. A. Electrochromism of NiO−TiO_2 Sol−Gel Layers. *J. Sol-Gel Sci. Techn.* **2006**, *39*, 195−206.
(33) Corrigan, D. A.; Knight, S. L. Electrochemical and Spectroscopic Evidence on the Participation of Quadrivalent Nickel in the Nickel Hydroxide. *J. Electrochem. Soc.* **1989**, *136*, 613−619.
(34) Chopoorian, J. A.; Dorion, G. H.; Model, F. S. Photochromism of Metal Oxides, I. The Light Sensitivity of MoO_3 or WO_3 Coprecipitated with TiO_2. *J. Inorg. Nucl. Chem.* **1966**, *28*, 83−88.
(35) He, T.; Yao, J. Photochromism in Composite and Hybrid Materials based on Transition Metal Oxides and Polyoxometalates. *Prog. Mater. Sci.* **2006**, *51*, 810−879.
(36) Kostecki, R.; Richardson, T.; McLarnon, F. Photochemical and Photoelectrochemical Behavior of a Novel TiO_2/$Ni(OH)_2$ Electrode. *J. Electrochem. Soc.* **1988**, *145*, 2380−2385.
(37) Fujishima, A.; Honda, K. Electrochemical Photolysis of Water at a Semiconductor Electrode. *Nature* **1972**, *238*, 37−38.
(38) Vinodgopal, K.; Kamat, P. V. Enhanced Rates of Photocatalytic Degradation of an Azo Dye using SnO_2/TiO_2 Coupled Semiconductor Thin Films. *Environ. Sci. Technol.* **1995**, *29*, 841−845.
(39) Hotchandani, S.; Kamat, P. V. Charge-Transfer Processes in Coupled Semiconductor System. Photochemistry and Photoelectrochemistry of the Colloidal CdS−ZnO System. *J. Phys. Chem.* **1992**, *96*, 6834−6839.
(40) Vindgopal, K.; Bedja, I.; Kamat, P. V. Nanostructured Semiconductor Films for Photocatalysis. Photoelectrochemical Behavior of SnO_2/TiO_2 Composite Systems and its Role in Photocatalytic Degradation of a Textile Azo Dye. *Chem. Mater.* **1996**, *8*, 2180−2187.
(41) Takahashi, Y.; Tatsuma, T. Oxidative Energy Storage Ability of a TiO_2−$Ni(OH)_2$ Bilayer Photocatalyst. *Langmuir* **2005**, *21*, 12357−12361.
(42) Takahashi, Y.; Tatsuma, T. Remote Energy Storage in $Ni(OH)_2$ with TiO_2 Photocatalyst. *Phys. Chem. Chem. Phys.* **2006**, *8*, 2716−2719.
(43) Zhang, W. K.; Wang, L.; Huang, H.; Gan, Y. P.; Wang, C. T.; Tao, X. Y. Light Energy Storage and Photoelectrochemical Behavior of the Titanate Nanotube Array/$Ni(OH)_2$ Electrode. *Electrochim. Acta* **2009**, *54*, 4760−4763.
(44) Huang, H.; Jiang, L.; Zhang, W. K.; Gan, Y. P.; Tao, X. Y.; Chen, H. F. Photoelectrochromic Properties and Energy Storage of $TiO_{2-x}N_x$/NiO Bilayer Thin Films. *Sol. Energy Mater. Sol. Cells* **2010**, *94*, 335−359.
(45) Zhang, L.; Xu, L.; Wang, J.; Shao, H.; Fan, Y.; Zhang, J. UV-Induced Oxidative Energy Storage Behavior of a Novel Nanostructured TiO_2−$Ni(OH)_2$ Bilayer System. *J. Phys. Chem. C* **2011**, *115*, 18027−18034.
(46) Pejova, B.; Kocareva, T.; Najdoski, M.; Grozdanov, I. Solution Growth Route of Nanocrystalline Nickel Oxide Thin Films. *Appl. Surf. Sci.* **2000**, *165*, 271−278.
(47) Cibrev, D.; Jankulovska, M.; Lana-Villarreal, T.; Gómez, R. Oxygen Evolution at Ultrathin Nanostructured $Ni(OH)_2$ Layers Deposited on Conducting Glass. *Int. J. Hydrogen Energy* **2013**, *38*, 2746−2753.
(48) Kim, K. S.; Winograd, N. X-ray Photoelectron Spectroscopic Studies of Nickel−Oxygen Surfaces Using Oxygen and Argon Ion bombardment. *Surf. Sci.* **1974**, *43*, 625−643.
(49) Greijer Agrell, H.; Boschloo, G.; Hagfeldt, A. Conductivity Studies of Nanostructured TiO_2 Films Permeated with Electrolyte. *J. Phys. Chem. B* **2004**, *108*, 12388−12396.
(50) Wang, H.; He, J.; Boschloo, G.; Lindström, H.; Hagfeldt, A.; Lindquist, S. E. Electrochemical Investigation of Traps in a Nanostructured TiO_2 Film. *Phys. Chem. B* **2001**, *105*, 2529−2533.
(51) Berger, T.; Monllor-Satoca, D.; Jankulovska, M.; Lana-Villarreal, T.; Gómez, R. The Electrochemistry of Nanostructured Titanium Dioxide Electrodes. *ChemPhysChem* **2012**, *13*, 2824−2875.
(52) Lide, D. R. *Handbook of Chemistry and Physics*; CRC Press: Boca Raton, FL, 2000; pp 8−21.
(53) Highfield, J. G.; Grätzel, M. Discovery of Reversible Photochromism in Titanium Dioxide using Photoacustic Spectroscopy. Implications for the Investigation of Light-Induced Charge-Separation and Surface Redox Processes in Titanium Dioxide. *J. Phys. Chem.* **1988**, *92*, 464−467.
(54) Kamat, P. V.; Bedja, I.; Hotochandani, S. Photoinduced Charge Transfer between Carbon and Semiconductor Clusters. One-Electron Reduction of C60 in Colloidal TiO_2 Semiconductor Suspensions. *J. Phys. Chem.* **1994**, *98*, 9137−9142.
(55) Monllor-Satoca, D.; Gómez, R. Electrochemical Method for Studying the Kinetics of Electron Recombination and Transfer Reactions in Heterogeneous Photocatalysis: The Effect of Fluorination on TiO_2 Nanoporous Layers. *J. Phys. Chem. C* **2008**, *112*, 139−147.
(56) Jankulovska, M.; Berger, T.; Lana-Villarreal, T.; Gómez, R. Trap States in TiO_2 Films made of Nanowires, Nanotubes, or Nanoparticles: An Electrochemical Study. *Electrochim. Acta* **2012**, *62*, 172−180.
(57) Jankulovska, M.; Barceló, I.; Lana-Villarreal, T.; Gómez, R. Improving the Photoelectrochemical Response of TiO_2 Nanotubes upon Decoration with Quantum-Sized Anatase Nanowires. *J. Phys. Chem. C* **2013**, *117*, 4024−4031.